Motion of a Cable Used as a Mooring

Harry E. Williams*
Harvey Mudd College, Claremont, Calif.

The equations governing the motion in a vertical plane of a heavy cable in a fluid are derived and applied to the problem of determining the tension in a cable that is fixed at the bottom and given a harmonic displacement of the upper end tangent to the undeformed cable. An order of magnitude analysis reveals the existence of a boundary layer near each end within which the spacial variations of the transverse dynamic displacement component varies rapidly compared with the spacial variation outside this region. For a range of parameters in which the Froude number (N_F) is negligible in comparison to the hydrodynamic drag number (N_D), the temporal variation of the dynamic tension is shown to be described by a first-order, nonlinear, ordinary differential equation. This equation has been solved both numerically and analytically using the Galerkin method giving results which are in very good agreement. Finally, the numerical results are compared with experiment and shown to be in good agreement. Thus, a relatively simple formula can be used to describe this type of dynamic behavior.

Nomenclature

A	= amplitude of disturbance at free end of the cable
C_D	= drag coefficient
d	= diameter of cable
E	= Young's modulus of cable
$\bar{E}$	$= \pi d^2 EA/4\mu g\ell^2$
e_s, e_n	= unit vectors directed parallel, perpendicular to the undeformed cable
e_s,e_n	= unit vectors directed parallel, perpendicular to the deformed cable.
f	= perturbed tension variable
g	= acceleration of gravity
ℓ	= unstretched length of cable
N_D	$= \rho_w A^2\omega^2 d/\mu g$
N_F	$= A\omega^2/g$
R	= radius of curvature of the inextensible cable
s	= arc length measured along the inextensible cable
$\bar{s}$	$= s/\ell$
t	= time variable
$\bar{t}$	$= \omega t$
T	= tension in the cable
$\bar{T}$	= reduced tension $(T/\mu g\ell)$
$\bar{T}_0$	= reduced tension in the inextensible cable
u, v	= displacement components along s, n directions
$\hat{u}$, $\hat{v}$	= dimensionless displacement components describing the CSS
$\tilde{u}$, $\tilde{v}$	= dimensionless displacement components describing the dynamic configuration
ϵ_1	$= 4\mu g\ell/\pi d^2 E$
ϵ_2	$= (A/\ell)^{1/2}$
ϵ	$= (u' - \ell v/R)/\ell$
θ_0	= slope of the inextensible cable
μ	= mass/length of cable
$\rho_w \rho_s$	= mass density of the fluid, cable
ω	= frequency of vibration
γ	$= (v' + \ell u/R)/\ell$
$(\dot{})$	$= \partial(\,)/\partial\bar{t}$
$(\,)'$	$= \partial(\,)/\partial\bar{s}$

Introduction

With the renewed emphasis on finding new sources of oil under the ocean, it has become increasingly important to be able to predict more of the factors influencing the effectiveness of drilling systems. One of the most important components of a drilling system is the mooring. Obviously, the design of the mooring must start with an analysis of a single mooring line. It is the purpose of this paper to explore the factors influencing the behavior of a mooring line which holds a moving point on the surface to a point on the bottom—a single point mooring.

A comprehensive review of investigations on the prediction of the motion of a cable under hydrodynamic loading has been given by Casarella and Parsons.[1] They also include a critical evaluation of the analytical models for the hydrodynamic forces acting on the cable. Recently, Choo and Casarella[2] re-examined this problem and presented expressions for the normal and tangential components of hydrodynamic resistance as functions of Reynolds number based on the velocity component perpendicular to the axis of the cable.

The problem of the dynamic response of a cable and its relation to the problem of determining the tension in a mooring system has been discussed by Wilson and Garbaccio.[4] They also present a solution of the equations of motion as presented by Langer,[5] obtained by the method of characteristics, which suggests that an approximate solution based on a pseudo-static analysis gives reasonable agreement for a specific example of wave motion. The approximation is based on neglecting the dynamic effects entirely (inertia and damping) and computing the tension in the cable (including the effect of linear elasticity) that is instantaneously in equilibrium given the appropriate displacement at the surface point. This method can also account for the effect of a portion of the cable lying on the seabed.

Subsequently, Nath and Felix,[6] following the solution proposed by Wilson and Garbaccio,[4] obtained solutions for the tension in and the displacements of a buoy-cable system. They rejected the pseudo-static analysis technique for the cable as not applicable for moorings in deep water. Further, they included a piece-wise linear stress-strain law in their calculations.

In a recent paper, Chang and Pilkey[7] describe a number of types of solution techniques for the single point mooring system. They note that very little progress has been made in obtaining analytical solutions, and discuss the relative merits of such numerical methods as: the finite element method, the finite difference method and the method of incremental integration.

The lack of analytical solutions stems from the nonlinear character of the problem. Even when the problem is idealized as two-dimensional and the stress-strain law is taken to be linear, the quadratic nature of the hydrodynamic damping force renders the governing equations nonlinear.

Received June 5, 1974; revision received February 11, 1975.
Index category: Marine Mooring Systems and Cable Mechanics.
*Professor of Engineering.

Some analytical results have been obtained by Nath[8] and extended by Smith and Nath[9] for the vertical mooring line excited by a vertical displacement or force prescribed at the upper end. This problem is tractible due to the absence of transverse motion and the attendant quadratic hydrodynamic force. It should be noted that their results are limited to the range of excitation such that the tension in the cable is always positive.

Of the purely numerical approaches, the finite element method, which is based on discretizing the otherwise continuous system, has received a great deal of attention lately due to its versatility in being able to account for both geometric and physical nonlinearities. Paul and Soler[10] used a discrete model to predict the two-dimensional trajectory of a towed body. They consider the cable as inextensible and neglect inertia effects (save for starting and stopping) as the motion is sufficiently slow. Dominguez and Smith[11] also discretize the system and present the governing equations in matrix form which is amenable to modal analysis. The damping is treated as an external force so the equations appear linear. A discrete model was used recently[12] by McLauchlan, Sanders, Taylor, and Collier to predict the snap loading conditions of very nearly vertical cable-mass systems.

The purpose of the present paper is to re-examine the governing equations for a single point mooring in the hope that, with suitable nondimensional variables, additional progress might be made toward obtaining the tension in a cable with reasonable accuracy. It is felt that the approximate solution suggested by Wilson and Garbaccio[4] is not valid in the range of frequency and amplitude of excitation of interest here. As an alternative, a solution is proposed which seems to agree well with a limited number of experimental observations.

The equations of motion developed here are based on a coordinate system fixed to the catenary that is defined by the position of an undisturbed, inextensional cable. This in contrast to the equations proposed by Langer,[5] and used by both Wilson and Garbaccio,[4] and Nath and Felix,[6] which use a coordinate system based on the instantaneous position of the cable. The first system is essentially Lagrangian while the second system is Eulerian. It is hoped that some simplficiations result from this alternate choice of system.

Further, in deriving the equations of motion, we assume the cable to be heavy in comparison with the fluid in which it is moving. With this assumption the effect of buoyancy is explicitly omitted, though this effect could be readily introduced by assuming a reduced mass when accounting for gravity force. A more important effect of this assumption is that the dynamic behavior of the fluid appears only in the drag—and this force is taken perpendicular to the instantaneous tangent to the cable. Implicitly omitted are terms which account for the "effective mass" of the fluid that is being accelerated, or, following the recent work of Breslin,[13] the force acting on the cable in addition to the viscous drag due to the dynamic component of fluid pressure acting over the surface of the cable. Both these effects should be included in a general study, but are considered negligible in the mooring applications undertaken here.

Finally, a far more restrictive assumption in the mooring application is that the cable material is represented as having a linear tension vs strain relationship. This assumption has been discussed by Wilson,[14] who also suggested that a more reasonable assumption would be a bilinear tension vs strain relation. However, for computational purposes here, the linear relation is used throughout. In the final analysis, the applicability of the relation can only be decided by tests of a particular cable material and construction.

Once the governing equations have been established, they are applied to the problem of determining the motion in the vertical plane of a single point mooring excited by a harmonic displacement of the upper end parallel to the tangent to the undisturbed cable. This problem is a considerable simplification of the actual problem—motion of a cable due to a random displacement of the upper end in an arbitrary direction. The value of obtaining a solution to such an idealized problem is that it might give the designer a clue to the magnitude of the expected dynamic behavior if the sea state was dominated by waves of a single frequency. The final answer to the question of general behavior can only be obtained by a more complete analysis and a comparison with experiment. Apart from the random nature of the excitation, the restriction to tangential motion is guided by the experimental observation[15] that the tension induced in a cable that is excited transversely is much less than the tension induced in a cable that is excited tangentially. Thus, the problem is more realistic than appears at first glance, and the analysis should give useful results on which a designer might base his calculations.

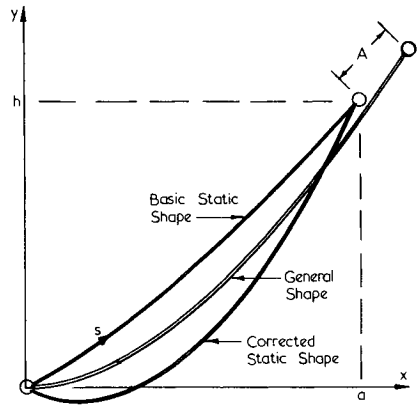

Fig. 1 Cable configuration.

Governing Equations

The equations governing the motion of a cable are the equations of motion and the tension-strain equation. These equations have been formulated in a number of ways differing chiefly with the choice of coordinate system. The choice is usually made to facilitate the description of a particular type of motion or boundary condition. It would also be advantageous if the choice of coordinate system allowed the assumption of small displacements to be made. As the motion studied here (see Fig. 1) is limited by the anchor at one end and a relatively small displacement of the upper end, it seems reasonable to expect that, under certain circumstances, deviations from the deformed static configuration might be small. Thus, in this paper, we will choose a coordinate system that is measured from the catenary form that is assumed by an inextensible cable acted on by its own weight and fixed at each end. This form will henceforth be referred to as the basic static shape (BSS) and is reviewed briefly in Appendix A.

It is also convenient to decompose the displacement field measured by the BSS into static and dynamic components. The static field describes the configuration of an elastic cable acted upon by its own weight and fixed at each end. This field will be referred to as the corrected static shape (CSS) and satisfies the equation of motion with time-varying terms deleted. The dynamic field satisfies the equations of motion and the boundary conditions that the lower end is fixed, and the upper end is displaced tangential to the cable end as described by the BSS.

In the following paragraphs, the governing equations are formulated in terms of a displacement field measured from the BSS using as independent variables the time t and the arc length s measured along the cable in the BSS. These equations are subsequently decomposed and used to generate the equations for the CSS and the dynamic field. First, however, it is necessary to formulate some kinematical relations regarding the description of the cable.

Assuming that the BSS has been established, we use this

framework to define the displacement of a point in the cable as

$$\delta = u(s,t)e_s + v(s,t)e_n \tag{1}$$

With reference to Fig. 2, let this displacement carry a line segment Δs in the BSS into the deformed line segment Δs^*, where

$$\Delta s^* = \Delta s + \delta(s+\Delta s/2,t) - \delta(s-\Delta s/2,t)$$

In terms of the strain, rotation variables ϵ, γ where

$$\epsilon = \partial u/\partial s - v/R \qquad \gamma = \partial v/\partial s + u/R \tag{2}$$

it follows that the deformed line segment can be written as

$$\Delta s^* = \Delta s + \Delta s(\epsilon e_s + \gamma e_n) + 0(\Delta s^2)$$

This expression can be used to generate the unit vectors e_s^*, e_n^* which are parallel and perpendicular, respectively, to the deformed configuration. In terms of the mechanical strain ϵ_s, where

$$\epsilon_s = \lim\ \Delta s \to 0\ \frac{\Delta s^* - \Delta s}{\Delta s} = (1+2\epsilon+\epsilon^2+\gamma^2)^{1/2} - 1 \tag{3}$$

it follows that

$$e_s^* = \lim\ \Delta s \to 0\ \Delta s^*/\Delta s^* = [(1+\epsilon)e_s + \gamma e_n]/(1+\epsilon_s) \tag{4a}$$

$$e_n^* = e_z \times e_s^* \tag{4b}$$

Further, for use later, it can be shown that

$$(1+\epsilon_s)\frac{de_s^*}{ds} = -e_s\left(\gamma/R - \frac{d\epsilon}{ds} + \frac{1+\epsilon}{1+\epsilon_s}\frac{d\epsilon_s}{ds}\right) + e_n\left(\frac{1+\epsilon}{R} + \frac{d\gamma}{ds} - \frac{\gamma}{1+\epsilon_s}\frac{d\epsilon s}{ds}\right) \tag{5}$$

With the kinematical description of the deformed cable established, we turn our attention to the equations of motion of a cable moving in a fluid in a vertical plane. It is assumed that the forces acting on an arbitrary element of the cable in the deformed state include a drag force perpendicular to the instantaneous tangent to the cable, the weight of the cable and the tension acting in the cable. Thus, we assume that 1) the effect of buoyancy is negligible, 2) the apparent mass of the fluid is negligible, and 3) the drag force parallel to the cable is negligible in comparison with the perpendicular component. Further, if we define the drag force per unit length of deformed cable as

$$D = -De_n^*, \quad D = \tfrac{1}{2}\rho_\omega C_D d \cdot \partial u^*/\partial t\,|\partial u^*/\partial t| \tag{6}$$

where $\partial u^*/\partial t$ is the velocity component along e_n^*, we are assuming that the hydrodynamic drag is instantaneously equal to its steady-state value at the same velocity. This assumption certainly represents a simplified description of the actual effect, but studies[1-3] seem to indicate that this model is a reasonable description of the drag force acting on slowly moving cables.

With these assumptions it follows from Fig. 2 that the net force acting on an element Δs^* of the deformed cable is

$$(Te_s^*)\,|_{s+\Delta s/2} - (Te_s^*)\,|_{s-\Delta s/2} - De_n^*\Delta s^* - \mu g \Delta s e_y \tag{7}$$

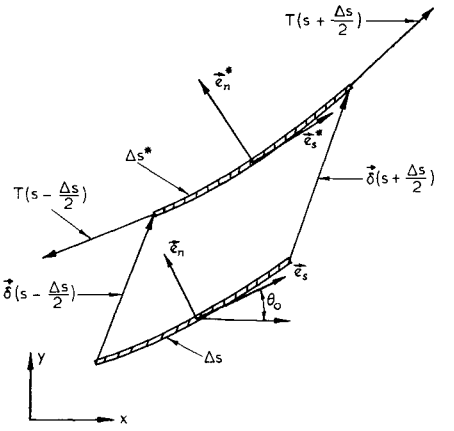

Fig. 2 Notation.

Now, taking the limit $\Delta s \to 0$ of Eq. (7) and setting it equal to the acceleration of a segment Δs of cable, we obtain the following equation of motion

$$\frac{\partial}{\partial s}(Te_s^*) - D(1+\epsilon_s)e_n^* - \mu g e_y = \mu\frac{\partial^2\delta}{\partial t^2} \tag{8}$$

We complete the set of equations with the addition of the tension-strain equation. Assuming that the cable is linearly elastic over the particular range of interest, we take

$$T = \frac{\pi d^2 E}{4}\epsilon_s \tag{9}$$

for a cable of diameter d and modulus E. Finally, we conclude this section with the displacement boundary conditions at each end that

$$u(0,t) = v(0,t) = v(\ell,t) = 0$$

$$u(\ell,t) = A\cos\omega t \tag{10}$$

where A is the amplitude of the driven end of the cable.

The Static Problem—The Corrected Static Shape

The first element of the displacement field to be studied is the static field of an elastic cable fixed at both ends. As the displacements are to be measured relative to the BSS, this configuration is then a measure of the effect of extensibility on the static configuration and is termed the corrected static shape (CSS). The governing equations for the CSS are Eqs. (8 and 9) with the time dependent terms omitted. Associated with these equations are the boundary conditions which require that the deflection components vanish at both ends ($s=0, \ell$).

In formulating the equations for the CSS, it is convenient to introduce the following dimensionless variables

$$T = \mu g \ell \bar{T} \qquad s = \ell\bar{s}$$

Anticipating that the CSS be near the BSS, we express the reduced tension $\bar{T}$ in terms of the reduced tension $\bar{T}_0$ of the BSS and a perturbation component f, where

$$\bar{T} = \bar{T}_0[1+f(\bar{s})]$$

Thus, the dimensionless form of the tension-strain equation [Eq.(9)] becomes

$$\bar{T}_0[1+f(\bar{s})] = \frac{\pi E d^2}{4\mu g \ell}\epsilon_s \tag{11}$$

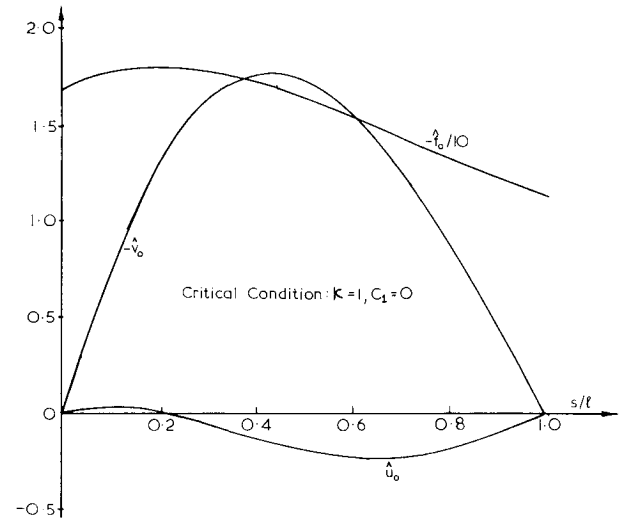

Fig. 3 Displacements and perturbed tension in the corrected static shape.

Assuming that $u,v=0(\delta)$, it follows from Eqs. (2 and 3) that $(\epsilon,\epsilon_s)=0(\delta/\ell)$, and from Eq. (11) that $\delta/\ell=0$ $(\mu g\ell/Ed^2)$. Thus, the solution for the CSS depends only on the parameter ϵ_1 where $\epsilon_1=(4\mu g\ell/\pi Ed^2)$. The parameter ϵ_1 can be identified as the average strain in the cable if the average tension in the cable is $\mu g\ell$. It is now apparent that the CSS will be near the BSS if $\epsilon_1 \ll 1$. In that follows, a solution of Eqs. (8 and 9) will be sought assuming $\epsilon_1 \ll 1$.

For $\epsilon_1 \ll 1$, we express the displacement, tension variables in the form

$$u=\epsilon_1 \ell \hat{u}(\bar{s},\epsilon_1)=\epsilon_1 \ell[\hat{u}_0(\bar{s})+0(\epsilon_1)] \tag{12}$$

$$v=\epsilon_1 \ell \hat{v}(\bar{s},\epsilon_1)=\epsilon_1 \ell[\hat{v}_0(\bar{s})+0(\epsilon_1)] \tag{13}$$

$$f=\epsilon_1 \hat{f}(\bar{s},\epsilon_1)=\epsilon_1[\hat{f}_0(\bar{s})+0(\epsilon_1)] \tag{14}$$

and seek the first term in the expansion to verify the solution process. The equations governing $\hat{u}_0$, $\hat{v}_0$, $\hat{f}_0$ are obtained by substituting Eqs. (12-14) into Eqs. (8 and 11) and taking the limit $\epsilon_1 \to 0$. The result of this process is the following set of equations.

$$\bar{T}_0=\hat{u}_0'(-\ell/R)\hat{v}_0 \tag{15}$$

$$(\hat{\gamma}_0\bar{T}_0)'+\hat{f}_0\cos\theta_0=0 \tag{16}$$

where

$$(\hat{f}_0\bar{T}_0)'\bar{\gamma}\cos\theta_0=0 \tag{17}$$

$$\hat{\gamma}_0=\hat{v}_0'+\ell\,\hat{u}_0/R \tag{18}$$

The solution to Eqs. (16 and 17) can be taken in the form

$$(\hat{f}_0,\hat{\gamma}_0)=\frac{B_1}{\bar{T}_0}[-\cos(\theta_0+B_2),\sin(\theta_0+B_2)] \tag{19}$$

With $\hat{\gamma}_0$ known, the displacements $\hat{u}_0$, $\hat{v}_0$ can be obtained from the simultaneous solution of Eqs. (15 and 18). The solution of Eqs. (15 and 18) that satisfies the boundary condition at $s=0$ is given by

$$\bar{T}_0\hat{u}_0=B_3\bar{s}+B_1\{C\sin B_2[\cosh(\bar{x}/c-c_1)$$

$$-\cosh c_1]-\bar{x}\cos B_2\}+\frac{3c^3}{2}\{\sinh(\bar{x}/c-c_1)$$

$$[1+\tfrac{1}{3}\sinh^2(\bar{x}/c-c_1)]+\sinh c_1[1+\tfrac{1}{3}\sinh^2 c_1]\} \tag{20}$$

The solution for $\hat{v}_0$ can now be obtained from Eqs. (15 and 20) and is given by

$$\frac{\ell}{R}\hat{v}_0=\frac{\bar{T}_0}{2}+[B_3-\hat{u}_0\sin\theta_0-B_1\cos(\theta_0+B_2)]/\bar{T}_0 \tag{21}$$

The constants of integration B_1, B_2, B_3 are determined from the remaining boundary conditions. Noting that it is really the combinations $\hat{B}_1=B_1\sin B_2$, $\hat{B}_2=B_1\cos B_2$ which appear in Eqs. (20 and 21), it follows from the boundary conditions that $\hat{B}_1$, $\hat{B}_2$, B_3 must satisfy

$$B_3-\hat{B}_2\operatorname{sech}c_1-\hat{B}_1\tanh c_1=-\tfrac{1}{2}\bar{T}_0^2(0)$$

$$B_3-\hat{B}_2\operatorname{sech}\kappa+\hat{B}_1\tanh\kappa=-\tfrac{1}{2}\bar{T}_0^2(1)$$

$$B_3+C\hat{B}_1(\cosh\kappa-\cosh c_1)-\frac{a}{\ell}\hat{B}_2$$

$$=-\frac{3C^3}{2}[\sinh\kappa(1+\tfrac{1}{3}\sinh^2\kappa)$$

$$+\sinh C_1(1+\tfrac{1}{3}\sinh^2 C_1)]$$

A numerical example is presented in Fig. 3 to illustrate the spacial behavior of the displacements and the perturbation tension.

The Dynamic Problem—Restriction to Small Strain

In this section, the general Eqs. (8 and 9) formulated earlier will be specialized by restricting attention to motion in which the strain, rotation components ϵ, γ can be taken small. We then wish to obtain a solution of these equations satisfying the boundary conditions [Eq. (10)].

In formulating the equations for motion with small strain, rotation, it is convenient to decompose the dependent variables into static and dynamic components defined by

$$u=u_{\text{css}}+u_{\text{dyn}} \qquad v=v_{\text{css}}+v_{\text{dyn}}$$

$$\epsilon=\epsilon_{\text{css}}+\epsilon_{\text{dyn}} \qquad \gamma=\gamma_{\text{css}}+\gamma_{\text{dyn}} \tag{22}$$

$$\bar{T}=\bar{T}_{\text{css}}+\bar{T}_{\text{dyn}}$$

where the subscripts identify either the CSS or the dynamic components. It then follows from the boundary conditions [Eq. (10)] and the boundary conditions for the CSS that the dynamic displacement components satisfy the following boundary conditions

$$u_{\text{dyn}}(0,t)=v_{\text{dyn}}(0,t)=v_{\text{dyn}}(1,t)=0 \tag{23}$$

$$u_{\text{dyn}}(1,t)=A\cos\omega t$$

These boundary conditions suggest that the following dimensionless variables be adopted

$$(u_{\text{dyn}},v_{\text{dyn}})=A(\tilde{u},\tilde{v}) \qquad f=\omega t$$

$$\epsilon_{\text{css}}=\epsilon_1(\hat{u}'-\frac{\ell}{R}\hat{v}) \qquad \gamma_{\text{css}}=\epsilon_1(\hat{v}'+\frac{\ell}{R}\hat{u}) \tag{24}$$

$$\epsilon_{\text{dyn}}=\frac{A}{\ell}(\tilde{u}'-\frac{\ell}{R}\tilde{v}) \qquad \gamma_{\text{dyn}}=\frac{A}{\ell}(\tilde{v}'+\frac{\ell}{R}\tilde{u})$$

Thus, we observe the appearance of the parameter A/ℓ in the formulation.

Before proceeding, we must determine a consistently accurate expression for the drag term D defined by Eq. (6). First, however, we need an expression for the local normal velocity component given by

$$\frac{\partial u^*}{\partial t} = \boldsymbol{e}_n^* \cdot \frac{\partial \delta}{\partial t}$$

For small rotation, strain, it follows from Eqs. (1, 4, and 24) that

$$\frac{\partial u^*}{\partial t} = A\omega[\dot{\tilde{v}} - \gamma\dot{\tilde{u}} + (\dot{\tilde{v}}, \dot{\tilde{u}})0(\epsilon^2)]$$

Thus, whenever the second term in this expression can be neglected, we obtain

$$D = \tfrac{1}{2}\rho_w C_D d A^2 \omega^2 \dot{\tilde{v}}|\dot{\tilde{v}}| \tag{25}$$

A preliminary set of equations can now be formulated for motion in which the strain ϵ, rotation γ are sufficiently small. First, a set of equations is obtained by substituting the decomposition defined by Eqs. (24) into Eqs. (8 and 9). These governing equations are expected to hold, of course, in general. However, the equations obtained from these equations by deleting all time dependent terms have already been solved and define the CSS. Thus, a considerably simplified form of the equations can be obtained from the general equations by subtracting the appropriate equations already satisfied by the CSS. The result of implementing this procedure is the following set of equations

$$\bar{T}'_{\text{dyn}}[1-\gamma^2/2+0(\epsilon^3)] - [\gamma_{\text{dyn}}(\bar{T}_{\text{dyn}}+\bar{T}_{\text{css}}) + \gamma_{\text{css}}\bar{T}_{\text{dyn}}]$$

$$\times \left[\frac{\ell}{R}(1-\epsilon) + \gamma' + 0(\epsilon^2)\right] + \bar{T}'_{\text{css}}[\tfrac{1}{2}\gamma_{\text{css}}^2 - \tfrac{1}{2}\gamma^2$$

$$+ 0(\epsilon^3, \epsilon_{\text{css}}^3)] + \gamma_{\text{css}} T_{\text{css}}\left[\frac{\ell}{R}\epsilon_{\text{dyn}} - \gamma'_{\text{dyn}} + 0(\epsilon^2)\right]$$

$$+ (\gamma_{\text{dyn}} + \gamma_{\text{css}})[1 + 0(\epsilon^3)] \cdot \frac{N_D C_D}{2}\dot{\tilde{v}}|\dot{\tilde{v}}| = N_F \ddot{\tilde{u}} \tag{26}$$

$$\bar{T}_{\text{dyn}} = \frac{\bar{E}\ell}{A}[\epsilon_{\text{dyn}} + \gamma^2/2 - \gamma_{\text{css}}^2/2 + 0(\epsilon^3, \epsilon_{\text{css}}^3)] \tag{27}$$

$$\bar{T}_{\text{dyn}}\left[\frac{\ell}{R}(1-\gamma^2/2) + \gamma' - (\gamma\epsilon)' + 0(\epsilon^3)\right]$$

$$+ \bar{T}_{\text{css}}\left[\gamma'_{\text{dyn}} + \frac{\ell}{2R}(\gamma_{\text{css}}^2 - \gamma^2)\right.$$

$$\left. + (\gamma_{\text{css}}\epsilon_{\text{css}})' - (\gamma\epsilon)' + 0(\epsilon^3, \epsilon_{\text{css}}^3)\right]$$

$$+ \gamma_{\text{css}}\bar{T}'_{\text{css}}[-\epsilon_{\text{dyn}} - \gamma^2/2$$

$$+ \gamma^2{}_{\text{css}}/2 + \epsilon^2 - \epsilon_{\text{css}}^2 + 0(\epsilon^3, \epsilon_{\text{css}}^3)] + [\gamma_{\text{dyn}}(\bar{T}_{\text{dyn}}' + \bar{T}_{\text{css}}')$$

$$+ \gamma_{\text{css}}\bar{T}'_{\text{dyn}}][1 - \epsilon - \gamma^2/2 + \epsilon^2 + 0(\epsilon^3)]$$

$$- [1 + \epsilon + 0(\epsilon^3)] \cdot N_D C_D/2 \cdot \dot{\tilde{v}}|\dot{\tilde{v}}| = N_F \ddot{\tilde{v}} \tag{28}$$

Thus, in addition to the parameters ϵ_1, A/ℓ, we observe the appearance of the additional parameters $\bar{E}$, N_D, N_F given by

$$\bar{E} = A/\ell\epsilon_1 \qquad N_D = \rho_w A^2\omega^2 d/\mu g \qquad N_F = A\omega^2/g \tag{29}$$

This implies that the solution of Eqs. (26-28) depends on four parameters ($\bar{E}$, N_D, N_F, A/l) as well as on $\bar{s}$, t. Though it is desirable to seek solutions for the complete range of the parameters, it is the purpose here to explore how Eqs. (26-28) might be simplified if we accept a limited range of parameters. In what follows, the range of parameters will be successively limited, and equations developed consistent with these limitations.

Approximate Forms of the Governing Equations

As experimental results reveal that $\bar{T}_{\text{dyn}} = 0(1)$ in the range of parameters of interest here, and Eq. (24) shows that $\epsilon_{\text{dyn}} = 0(A/\ell)$, we observe from Eq. that $\bar{E} = 0(1)$. Further, as we have already obtained a solution for the CSS for $\epsilon_1 \ll 1$ and wish to use this solution to construct the general solution, it follows from Eq. (29) that $A/\ell \ll 1$ if $\bar{E} = 0(1)$, $\epsilon_1 \ll 1$. Thus if we arbitrarily choose N_D, $N_F = 0(1)$, we proceed to seek solutions of Eqs. (26-28) for the range $A/\ell \ll 1$, $E = 0(1)$.

The limiting form of Eqs. (26-28) is obtained by substituting the strain, rotation expressions given by Eq. (24) and taking the limit $A/\ell \to 0$, $\bar{E}$-fixed. The result of this process is the following set of equations

$$\bar{T}_{\text{dyn}}\frac{\ell}{R} - \tfrac{1}{2}C_D N_D \dot{\tilde{v}}|\dot{\tilde{v}}| = N_F \ddot{\tilde{v}} \tag{30}$$

$$\bar{T}'_{\text{dyn}} = N_F \ddot{\tilde{u}} \tag{31}$$

$$\bar{T}_{\text{dyn}} = \bar{E}\left(\tilde{u}' - \frac{\ell}{R}\tilde{v}\right) \tag{32}$$

The character of Eqs. (30-32) can be seen if the tension is eliminated. Thus, with

$$\tilde{u}'' - \frac{N_F}{\bar{E}}\ddot{\tilde{u}} = \left(\frac{\ell}{R}\tilde{v}\right)'$$

$$\frac{N_F}{\bar{E}}\ddot{\tilde{v}} + \frac{C_D N_D}{2\bar{E}}\dot{\tilde{v}}|\dot{\tilde{v}}| + \left(\frac{\ell}{R}\right)^2\tilde{v} = \frac{\ell}{R}\tilde{u}' \tag{33}$$

we observe that the first equation is the wave equation with distributed loading, while the second has the appearance of the oscillator equation with damping and a forcing term. Coupling between the equations is removed whenever the BSS corresponds to the taut condition, i.e., $\ell/R = 0$. In this case, which has been extensively treated by Yamamoto et al. (16), the transverse displacement vanishes, and the tangential displacement is governed by the wave equation with a reduced wave speed given by $\bar{c}^2 = \bar{E}/N_F$.

Returning now to Eqs. (30-32), it is apparent that the order of the equations has been reduced in the limit process, and that we should not be able to enforce all the boundary conditions on the solution of Eqs. (30-32). This situation is typical of a singular perturbation process. We expect that a solution of Eqs. (30-32) be valid over $0 < \bar{s} < 1$, but require a boundary-layer analysis to develop equations valid near the end points ($s = 0, \ell$).

In such a boundary-layer analysis, we first need a suitable length scale. The form of Eqs. (26-28) suggests that a length scale in the neighborhood of $s = 0$ be chosen in the form

$$\bar{s} = \epsilon_2 \xi_0 \qquad \epsilon_2^2 = A/\ell$$

The strain, tension variables associated with the CSS in this region become

$$\epsilon_{\text{css}} = \epsilon_1[\hat{\epsilon}(0) + 0(\epsilon_2)]$$

$$\bar{T}'_{\text{css}} = \bar{T}'_{\text{css}}(0) + 0(\epsilon_2) \tag{34}$$

etc. Being mindful of the fact that the dynamic variables in the boundary layer must match the dynamic variables in the outer region, we look for a solution of Eqs. (26-28) in the form

$$\tilde{u}=\tilde{u}_{BL}^{(0)}(\xi_0, t; \bar{E}, N_D, N_F)+0(\epsilon_2) \tag{35a}$$

$$\tilde{v}=\tilde{v}_{BL}^{(0)}(\xi_0, t; \bar{E}, N_D, N_F)+0(\epsilon_2) \tag{35b}$$

$$\bar{T}_{dyn}=\bar{T}_{dyn,BL}^{(0)}(\xi_0, t; \bar{E}, N_D, N_F)+0(\epsilon_2) \tag{35c}$$

The boundary-layer form of Eqs. (26-28) is obtained by substituting Eqs. (34 and 35) and taking the limit $\epsilon_2 \to 0$, ξ_0-fixed. The result of this process if the following set of equations

$$\partial \tilde{u}_{BL}^{(0)}/\partial \xi_0=0 \tag{36}$$

$$\partial \bar{T}_{dyn,bl}^{(0)}/\partial \xi_0=0 \tag{37}$$

$$[\ \bar{T}_{dyn,BL}^{(0)}+\bar{T}_0(0)\ ]\ (\partial^2 \tilde{v}_{BL}^{(0)}/\partial \xi_0^2)+\bar{T}_{dyn,BL}^{(0)}(\ell/R)(0)$$

$$-\tfrac{1}{2}C_D N_D \dot{\tilde{v}}_{BL}^{(0)}|\dot{\tilde{v}}_{BL}^{(0)}|=N_F \ddot{\tilde{v}}_{BL}^{(0)}$$

We note that the tangential displacement and the dynamic tension in the boundary layer are functions of the time ($\bar{t}$) only: The specific form of $\bar{T}_{dyn,BL}^{(0)}(\bar{t})$ cannot be determined until the solution of Eqs. (30-32) is obtained. When this is accomplished, the boundary-layer tension is obtained, following the procedure developed by Cole.[17] by matching the boundary-layer solution with the solution in the outer region.

The form of $\tilde{u}_{BL}^{(0)}(\bar{t})$ is obtained from the boundary conditions that must be satisfied by the solution of the boundary-layer equations. As

$$\tilde{u}_{BL}^{(0)}(\xi_0=0,t)=\tilde{v}_{BL}^{(0)}(\xi_0=0,t)=\tilde{v}_{BL}^{(0)}(\xi_1=0,t)=0 \tag{39}$$

$$\tilde{u}_{BL}^{(0)}(\xi_1=0,t)=\cos t$$

it follows from Eq. (36) that

$$\tilde{u}_{BL}^{(0)}(\xi_0,t)=0 \tag{40}$$

The boundary-layer equations in the neighborhood of $\bar{s}=1$ are obtained in a similar manner. The length scale suitable near $\bar{s}=1$ can be shown to be

$$\bar{s}=1-\epsilon_2 \xi_1$$

and leads to a set of equations similar in form to Eqs. (36-38) (save that $\bar{T}_0(1)$, ℓ/R (1) appear as coefficients in place of $\bar{T}_0$ (0), ℓ/R (0)). Thus, it can be shown that the tangential displacement in the boundary layer at the top is also a function of time only, and that

$$\tilde{u}_{BL}^{(0)}(\xi_1, t)=\cos t$$

At this stage we leave the boundary-layer equations and direct our attention to the equations governing the outer solution.

A Solution of the Dynamic Problem for $N_F=0$

As the equations governing the outer solution, Eqs. (30-32) are nonlinear partial differential equations, it is probable that solutions can only be obtained by numerical means. The degree of difficulty, however, can be reduced considerably by further limiting the range of the parameters. In particular, if we take $N_F(=A\omega^2/g) \ll N_D$, some further progress is possible. Thus, in this section, we seek a solution of Eqs. (30-32, 36-38) in the limit $N_F \to 0$ assuming that

$$\tilde{u}=\tilde{u}(\bar{s}, \bar{t}; \bar{E}, N_D)+0(N_F)$$

$$\tilde{u}_{BL}^{(0)}=\tilde{u}_{BL}^{(0)}(\xi_0, \bar{t}; \bar{E}, N_D)+0(N_F) \text{ etc.}$$

The physical significance of the limit $N_F \to 0$, N_D-fixed can be understood if one rewrites the definition of the parameter N_D in the form

$$N_D=4/\pi(\rho_w/\rho_s)(A/d)N_F$$

Thus, the limiting condition can be achieved by making w small while A/d becomes large. This implies that we are studying a very slow motion with an amplitude that is much larger than the diameter of the cable.

A solution of Eqs. (30-32) as $N_F \to 0$ can be taken in the form

$$\tilde{v}=(\ell/R)^{1/2}F(\bar{t}) \tag{42}$$

$$\bar{T}_{dyn}=\tfrac{1}{2}C_D N_D \dot{F}|\dot{F}| \tag{43}$$

where

$$\tilde{u}'=\frac{C_D N_D}{2\bar{E}}\dot{F}|\dot{F}|+(\ell/R)^{3/2}\cdot F \tag{44}$$

The function $F(\bar{t})$ is determined by the matching principle requirement that the solution for the tangential displacement governed by Eq. (42) must be continuous at each end ($\bar{s}=0, 1$) with the appropriate boundary-layer solution Eqs. (40 and 41), i.e.,

$$\tilde{u}(\bar{s}\to 0,\bar{t})=0 \qquad \tilde{u}(\bar{s}\to 1, \bar{t})=\cos \bar{t}$$

These conditions allow us to integrate Eq. (44) to obtain

$$\tilde{u}(\bar{s},\bar{t})=F(\bar{t})\int_0^{\bar{s}}(\ell/R)^{3/2}dx+\frac{C_D N_D}{2\bar{E}}\dot{F}|\dot{F}|\bar{s} \tag{45}$$

in general, and

$$\tilde{u}(1,\bar{t})=\lambda F+\frac{C_D N_D}{2\bar{E}}\dot{F}|\dot{F}|=\cos \bar{t} \tag{46}$$

in particular. The integral λ is defined in Appendix A. This latter equation is used to define $F(\bar{t})$. Once periodic solutions of this equation are found, the solution in the outer region is complete as the transverse displacement and the dynamic tension are determined from Eqs. (42 and 43).

Periodic solutions of Eq. (46) have been obtained for a variety of parameters N_D, $\bar{E}$ and are presented in Figs. 4 and 5. The solutions were obtained using the subroutine RKGS (Runge-Kutta-Gill) available from IBM, Inc. The technique was to make an initial guess for $F(0)$ and compute $F(2\pi)$. This process was repeated until $F(0)$, $F(2\pi)$ were identical.

The form of the solutions presented in Figs. 4 and 5 suggests that the function $F(\bar{t})$ is nearly a displaced sine wave. An approximate solution of Eq. (46) has been obtained making use of this observation and using the Galerkin averaging technique. The results agree very closely with the numerical solution described previously. The details of this

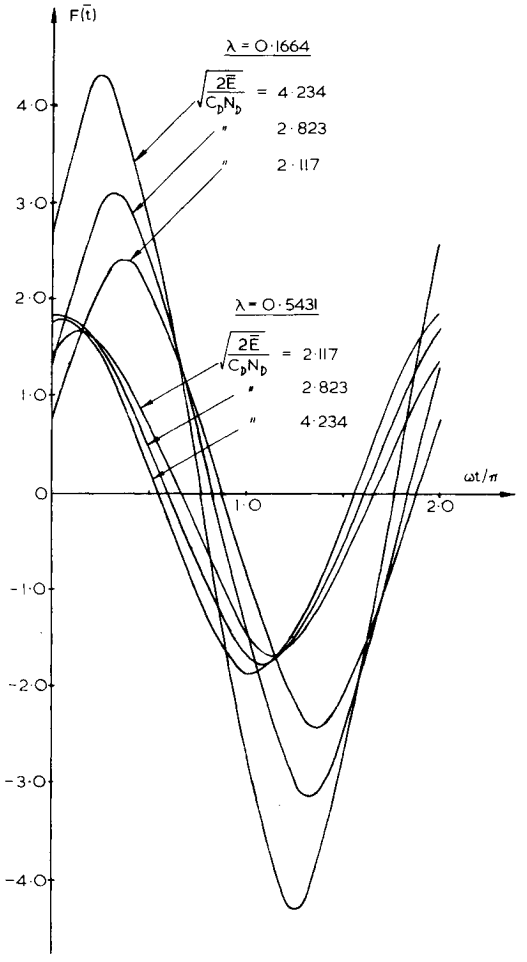

Fig. 4 Time dependency of transverse displacement.

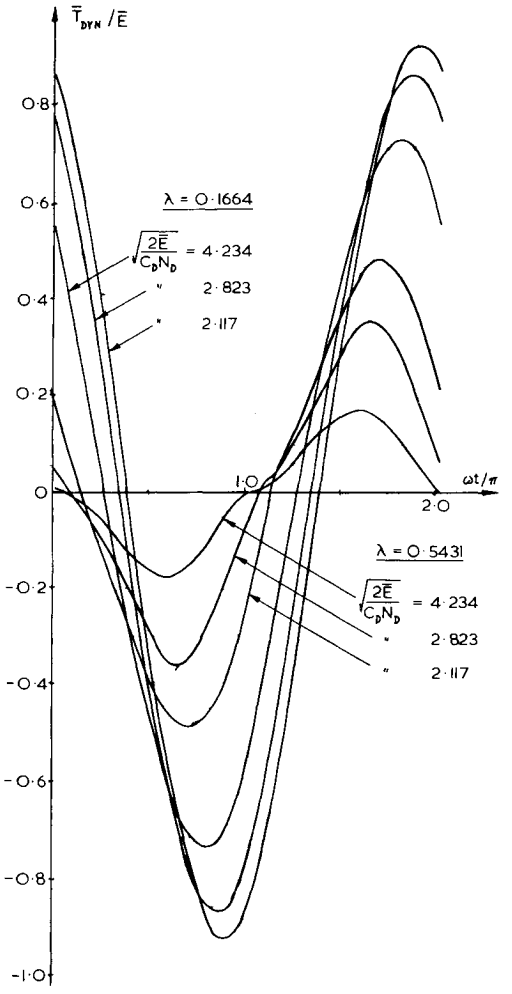

Fig. 5 Time dependency of reduced dynamic tension.

solution and a comparison with the Runge-Kutta-Gill solution are presented in Appendix B.

With the outer solution now completely defined, we return to the boundary-layer equations and seek a solution for the dynamic tension and the transverse displacement. Using the argument previously used for the tangential displacement, we conclude that the dynamic tension in the boundary layer is a function of time only and that

$$\bar{T}^{(0)}_{\mathrm{dyn,BL}}(\xi_0,\bar{t}) = \bar{T}_{\mathrm{dyn}}(\bar{s}\to 0,\bar{t});$$

$$\bar{T}^{(0)}_{\mathrm{dyn,BL}}(\xi_1,\bar{t}) = \bar{T}_{\mathrm{dyn}}(\bar{s}\to 1,\bar{t})$$

However, as $\bar{T}_{\mathrm{dyn}}$ is itself a function of time only, we conclude that

$$\bar{T}^{(0)}_{\mathrm{dyn,BL}} = \bar{E}(\cos t - \lambda F) \tag{47}$$

in both boundary layers.

Finally, the transverse deflection in the boundary layer must be obtained. Specifically, we seek a solution of Eq. (38) (with $N_F = 0$) subject to the boundary conditions given by Eqs. (39) that matches the solution in the outer region given by Eq. (42) in the region of overlap, i.e.,

$$\text{limit as } \xi_0\to\infty \quad \bar{v}^{(0)}_{\mathrm{BL}}(\xi_0,\bar{t}) = (\ell/R(0))^{1/2}\cdot F(\bar{t}) \tag{48}$$

This solution is required to verify the applicability of the singular perburbation procedure to this problem. The main problem is to verify the existence of solutions of Eq. (38) that tend to the required limit [Eq. (48)] as $\xi_0\to\infty$. If such a solution cannot be found, the entire solution process is of doubtful validity.

The task of obtaining the required solution of Eq. (38) is a difficult one requiring, at least, a relatively sophisticated numerical technique. We propose here to adopt an alternative task, and seek only an approximate solution. If such can be found, we will conclude that an exact solution could probably be found and that the solution process was valid. The exact form of the transverse displacement is not actually required, as an approximate solution is all that is required for an indication of the physical behavior of the cable near the ends. To that end, it can be shown (see Appendix C) that an approximate solution of Eq. (38) does exist that satisfies both the boundary condition at the end and the matching condition. This solution was obtained by numerically integrating an ordinary differential equation obtained from Eq. (38) by the Galerkin averaging technique. The details of this method and the solution are presented in Appendix C.

Discussion and Comparison with Experiment

In the preceding sections, a solution has been found for a particular range of parameters such that the small strain restriction could be applied and inertial effects ignored. The solution required that a singular perturbation sequence be constructed and shown to be consistent. Though this latter point has not been conclusively proved, it has been shown to be plausible by recourse to approximate methods. Further, it

Table 1 Comparison of calculated and experimental results for peak dynamic tension[a]

ω_p (rad/sec)	λ	N_D	N_F	$\bar{T}_0(1)$	$\bar{T}_{\text{dyn,max}}$	$\frac{T_p(\text{calc})}{T_p(\text{exp})}$ max
0.50	0.5431	0.2137	0.03882	1.626	0.663	0.90
0.75		0.4808	0.08735		1.25	0.94
1.00		0.8547	0.1553		1.86	1.05
0.50	0.1664	0.2137	0.03882	3.252	2.85	1.10
0.75		0.4808	0.08735		3.34	1.14
1.00		0.8547	0.1553		3.57	1.19

[a] $A_p = 5$ft, $\ell_p = 2555$ ft, $h_p = 1000$ ft, $\bar{E} = 3.831$, $C_D = 2.0$.

should be noted that the sequence defined by Eq. (35) (and an associated sequence appropriate to the outer solution) could be continued to obtain further accuracy if desired.

At this stage, however, it seems advisable to evaluate the existing results by a comparison with experiment. Such verification can be provided in a limited way by referring to a series of experiments performed at the author's institution under the sponsorship of the Western Offshore Drilling and Exploration Company.† A report describing this work and presenting the variation of peak dynamic tension as a function of amplitude and frequency of excitation and cable geometry was prepared[15] and is cited here as evidence of the applicability of the analysis. A brief description of the relevant test procedure is given.

The cable orientation during the tests was similar to that sketched in Fig. 1. In particular, the upper end of the cable was positioned prior to each test so that no portion of the cable ever came into contact with the bottom. Excitation of the upper end was provided by driving a slider-crank mechanism with an electric motor whose frequency could be varied and controlled. The slider could be oriented to drive the cable either parallel to or perpendicular to the BSS. The tension in the cable was sensed by connecting the end of the cable to the slider through the flexible link on which an electric resistance strain gage was mounted. The output of the gage was recorded on a strip chart recorder. Thus, the stroke of the slider, the frequency of excitation, and the amplitude of the tension at the end of the cable could be simultaneously recorded.

The cable used in the tests reported here was a 0.025 in. diam (1×7 construction) stainless steel cable manufactured by Seven Strand Tackle Manufacturing Co. The elasticity of the system was adjusted by placing a coil spring in series with the cable at the bottom support point. This adjustment was made to study a scaling law that had been proposed by WODE and was an attempt to model the behavior of a much stiffer prototype. This method of obtaining elastic similarity was suggested by Collier[18] as a means for simultaneously reproducing the appropriate stiffness and hydrodynamic drag required of a model.

A comparison of experimental and calculated results for maximum dynamic tension is presented in Table 1. The calculated results are also presented in Figs. 4 and 5. For convenience in referring the parameters to a prototype configuration, the cable geometry, the amplitude and the frequency of excitation are referred to prototype values. The relations between model and prototype parameters is expressed in terms of a scale factor s and given by $A_m = A_p/s$, $\omega_m^2 = s\omega_p^2$, $\ell_m = \ell_p/s$, $T_m = T_p/s^3$, and $h_m = h_p/s$. The scale factor for the tests reported here is $s = 100$.

For the range of amplitude and frequency covered in Table 1, the comparison between theory and experiment seems to be satisfactory. It is felt that the degree of agreement indicates the general applicability of the theory, and that the disagreement may be within the range of uncertainty of the experimental data or be due to an incorrect choice of the physical parameters that appear in the theory. Unfortunately, it is not possible at this writing to estimate the range of uncertainty of the data as error bars were not included in Ref. 15. As to the choice of parameters, many, like the effective Young's Modulus of the cable material, were obtained by testing and are reasonably well defined. However, it should be noted that the drag coefficient (C_D) was arbitrarily taken to be 2.0 for all calculations based on Eqs. (46) and (47). This number represents an estimate of the average drag coefficient that might be expected over the range of Reynold's numbers expected in the tests (based on excitation velocity). In future work, it might be a more reasonable choice to pick a C_D based on an average velocity taken over the length of the cable.

It should be noted that an apparent slack condition existed in 3 of the 6 configurations tested; i.e., the dynamic tension exceeded the static tension thereby producing a compression in the cable during a portion of the cycle. This behavior was also noted for the present cable configuration at larger values of amplitude and frequency reported in Table 1; i.e.,

$$T_{\text{calc}}/T_{\text{exp}} = 1.79 \text{ @ } A_p = 15 \text{ ft}, \omega_p = 1 \text{ rad/sec}$$

It appears from the data that $T_{\text{calc}}/T_{\text{exp}}$ increases as $T_{\text{dyn,max}}/T_o(1)$ increases. Thus, the theoretical behavior seems to deviate further from the observed behavior when the slack condition exists for a greater portion of the cycle. However, provided that the cable remains in tension throughout the cycle, the present analysis seems to give results which are in reasonable agreement with experiment.

It is apparent that further work is required to cover that range of parameters in which the slack condition exists and also to develop a theory to account for motion in which some of the cable lies on the bottom during a portion of the cycle. In both these areas, the excitation should be taken parallel to the BSS, as it has been observed[15] that transverse excitation produces a dynamic tension for the same amplitude and frequency which is small in comparison with the tension associated with parallel excitation.

Further, the effect of the Froude number (N_F) on the motion should be investigated. Though the range of parameters of interest to designers of large mooring systems may not, as yet, lead to values of N_F comparable with N_D, one should anticipate other applications of this theory in which both parameters are comparable.

Finally, the use of a coil spring to adjust the elasticity of the cable should be justified through further experiment. Though this technique seems reasonable in light of the aforementioned result that the dynamic tension is, to a first approximation, independent of position, the question should be answered in a definitive way.

Appendix A—The Governing Equations of the Basic Static Shape

The position of the cable in the BSS is described in terms of the arc length(s) measured along the cable from the lower end. There is attached at each point along the cable a set of unit vectors $\boldsymbol{e}_s$, $\boldsymbol{e}_n$ which define the local tangential, perpendicular directions, respectively. The orientation of these unit vectors is measured by the angle θ_0. Associated with the coordinate s,

†The author is indebted to G.B. Bergman, Sr. Vice President, W.O.D.E., for permission to publish these data.

and the angle θ_0 is the local radius of curvature R where $R=ds/d\theta_0$. If we adopt the convention that $\boldsymbol{e}_n=\boldsymbol{e}_z\times\boldsymbol{e}_s$, it follows that

$$d/ds(\boldsymbol{e}_s, \boldsymbol{e}_n)=(\boldsymbol{e}_n, -\boldsymbol{e}_s)/R$$

The equations governing the BSS are the equilibrium equations obtained from Eq. (8) by replacing $\boldsymbol{e}_s^*$, $\boldsymbol{e}_n^*$ by $\boldsymbol{e}_s$, $\boldsymbol{e}_n$, respectively, and by deleting the velocity and acceleration. Expressed in terms of the reduced tension $\bar{T}_0$ and are length, they are

$$(\bar{T}_0\boldsymbol{e}_s)'-\boldsymbol{e}_y=0$$

These equations are readily integrated to give the spacial variation of the tension and the shape of the cable.

If the cable does not sag down from the anchor, i.e., sin $\theta_0\geqslant 0$, it can be shown that

$$\bar{y}=c[\cosh(\bar{x}/c-c_1)-\cosh c_1]$$

$$\bar{s}=c[\sinh(\bar{x}/c-c_1)+\sinh c_1]$$

$$\bar{T}_0=c\cosh(\bar{x}/c-c_1)$$

$$\ell/R=\cos\theta_0/\bar{T}_0=(1/c)\,\operatorname{sech}^2(\bar{x}/c-c_1)$$

where $c=\bar{T}_0\cos\theta_0$.

In a typical mooring design, the length of the cable ℓ, the depth of anchor h, and the tension at the upper end $\bar{T}_0(1)$ might be given. If we define a parameter κ, where $\kappa=a/c\ell-c_1$ it can be shown that

$$\tanh\kappa=\frac{h}{\ell}+\frac{1-(h/\ell)^2}{2\bar{T}_0(1)}$$

With κ so determined, the constants c, c_1 follow from the relations that express the fact that the tension is prescribed at the upper end; i.e.,

$$c=T_0(1)/\cosh\kappa$$

and that $\bar{s}=1@x=a$, i.e., $\sinh c_1=\cosh\kappa/\bar{T}_0(1)-\sinh\kappa$. It immediately follows that

$$\frac{\ell}{R}(0)=\frac{\operatorname{sech}^2 c_1}{c}\qquad \bar{T}_0(0)=c\cosh c_1$$

$$\frac{\ell}{R}(1)=\frac{\operatorname{sech}^2\kappa}{c}\qquad \bar{T}_0(0)=c\cosh\kappa$$

Of particular interest in the solution for the dynamic displacement is the integral

$$I(s)=\int_0^s\left[\frac{\ell}{R}(\xi)\right]^{3/2}d\xi$$

Using the expression for ℓ/R previously given, it can be shown that

$$I(s)=[\tanh(\bar{x}/c-c_1)+\tanh c_1]/(c)^{1/2}$$

In particular, we define

$$\lambda=I(1)=\frac{1}{(c)^{1/2}}(\tanh\kappa+\tanh c_1)$$

Appendix B—Approximate Solution for Tangential Displacement Function

Although it is a comparatively simple matter to obtain periodic solutions of Eq. (46) using the subroutine RKGS, it would be useful to obtain an approximate analytical solution as then the explicit dependency of the characteristics of the motion on the parameters of the system can be examined. Thus, in the following section, a solution of Eq. (46) will be developed using the Galerkin averaging technique based on the observation (see Figs 4 and 5) that the solutions obtained using RKGS are very nearly displaced sine waves.

If the form of the soluton for $F(\bar{t})$ is expressed in terms of coefficients A,B in the form

$$F(t)=A\sin t+B\cos t \tag{B1}$$

then, following the Galerkin procedure, the numerical values of A, B can be determined from the requirement that the error function $\epsilon(t)$ be orthogonal to both the basis functions (sin t, cos t). The error function is defined as the nonzero remainder appearing in Eq. (46) when the approximate form of the solution for $F(t)$ is substituted. Thus with

$$\epsilon(t)=\lambda(A\sin t+B\cos t)-\cos t+\frac{C_DN_D}{2\bar{E}}(A\cos t - B\sin t)\cdot|A\cos t-B\sin t| \tag{B2}$$

the coefficients A, B follow from the requirements that

$$\int_0^{2\pi}dt\,\epsilon(t)\,(\sin t,\cos t)=0 \tag{B3}$$

If the coefficients A, B are replaced by $\bar{A}$, $\bar{B}$. where

$$(\bar{A},\bar{B})=\lambda(A,B)$$

it follows that the requirements expressed by Eqs. (B2) lead to the following equations for $\bar{A}$, $\bar{B}$

$$\bar{A}=C_0\bar{B}(\bar{A}^2+\bar{B}^2)^{1/2}$$

$$\bar{B}+C_0\bar{A}(\bar{A}^2+\bar{B}^2)^{1/2}=1 \tag{B4}$$

where $C_0=4C_DN_D/3\pi\lambda^2\bar{E}$. Further, in terms of the angle α, where

$$\sin\alpha=A/(A^2+B^2)^{1/2},\quad \cos\alpha=B(A^2+B^2)^{1/2}$$

and an amplitude $\bar{F}_0$ defined by

$$\bar{F}_0=(\bar{A}^2+\bar{B}^2)^{1/2}>0$$

we obtain Eqs. (B4) in the alternate form

$$C_0\bar{F}_0=\tan\alpha$$

$$C_0\bar{F}_0^2\sin\alpha+\bar{F}_0\cos\alpha-1=0 \tag{B5}$$

Eliminating $\bar{F}_0$ from Eq. (B5) leads to

$$C_0\cos\alpha=\tan\alpha \tag{B6}$$

Table 2 Comparison of solutions of Eq. (46) for $\bar{E}=3.831$ and $C_D=2.0$.

λ	N_D	α_0	$F(t)\|_{max}$		$(\bar{T}_{dyn}/\bar{E})\|_{max}$	
			Eqs. (B7)	RKGS	Eq. (B9)	RKGS
0.5431	0.2137	8.95°	1.819	1.839	0.1845	0.1730
	0.4808	18.8°	1.743	1.800	0.3811	0.3315
	0.8547	29.2°	1.607	1.689	0.5759	0.4842
0.1664	0.2137	48.5°	3.979	4.305	0.8832	0.7377
	0.4808	61.5°	2.872	3.149	1.035	0.8700
	0.8547	68.4°	2.216	2.431	1.095	0.9247

Thus, once α is determined, we can write

$$F(t)=\frac{\bar{F}_0}{\lambda}\cos(t-\alpha)=\frac{\cos\alpha}{\lambda}\cos(t-\alpha) \tag{B7}$$

as $\bar{F}_0=\cos\alpha>0$. This last relation can be used to identify the correct solution for α.

The roots α of Eq. (B6) can be seen from a plot of the right and left-hand sides of Eqs. (B6) to lie in the first and second quadrants of the region $0\leqslant\alpha\leqslant 2\pi$. Further, accounting for periodicity, it can be observed that $\alpha\pm 2n\pi$ (n-integral) are also roots. However, as $\cos\alpha>0$, and no new information is obtained from the solution corresponding to n-arbitrary, it is concluded that $\alpha=\alpha_0$ is the correct solution where

$$\cos\alpha_0=\left[(1+4C_0^2)^{1/2}-1\right]^{1/2}/(\sqrt{2}C_0) \tag{B8}$$

Of particular interest is the amplitude of the dynamic tension predicted by this simplfied analysis. In dimensional terms, it follows that

$$T_{dyn,max}=\frac{C_D}{2}\left[\frac{\cos\alpha_0}{\lambda}\right]^2\rho_\omega\ell d(A\omega)^2 \tag{B9}$$

For small values of α_0, it can be seen that the dynamic tension varies as the square of both the amplitude (A) and the frequency (ω), and linearly with the length (ℓ) and the diameter (d) of the cable.

The results of calculation based on Eq. (B8) are presented in Table 2 along with corresponding values obtained by numerical integration of Eq. (46). It is apparent that agreement is satisfactory over the range of parameters studied.

Appendix C—Approximate Solution of the Boundary-Layer Equation

In this section, the Galerkin averaging technique that was used in Appendix B to solve Eq. (46) will be used to reduce Eq. (38) from a partial differential equation to an ordinary differential equation. A solution to the ordinary differential equation can then be obtained by numerical integration.

If we limit the range of the parameters such that a satisfactory solution of Eqs. (46) can be taken in the form

$$F(t)=F_0\cos\tau \qquad (F_0>0)$$

where $\tau=t-\alpha_0$, and

$$\bar{T}_{dyn}=-\frac{C_DN_D}{2}F_0^2\sin\tau|\sin\tau|$$

we can rewrite the boundary-layer equation [Eq. (38)] as

$$\frac{F_0}{(\ell/R)(0)^{1/2}}\left[\frac{2\bar{T}_0(0)}{C_DN_DF_0^2}-\sin\tau|\sin\tau|\right]\frac{\partial^2V}{\partial\xi_0^2}-\sin\tau|\sin\tau|-\frac{\partial V}{\partial\tau}\left|\frac{\partial V}{\partial\tau}\right|=0 \tag{C1}$$

Here, we have introduced, for convenience, the normalized displacement function defined by

$$\tilde{v}_{BL}^{(0)}(\xi_0,\tau)=\left(\frac{\ell}{R}(0)\right)^{1/2}F_0V(\xi_0,\tau)$$

We require further that

$$V(0,\tau)=0 \qquad \lim_{\xi_0\to\infty}V(\xi_0,\tau)=\cos\tau \tag{C2}$$

In constructing approximate equations to replace Eq. (C1), it is convenient to decompose $V(\xi_0,\tau)$ as follows

$$V(\xi_0,\tau)=V_1(\xi_0)\sin\tau+V_2(\xi_0)\cos\tau$$

$$=(V_1^2+V_2^2)^{1/2}\cos[\tau-\alpha(\xi_0)] \tag{C3}$$

The component functions V_1, V_2 must also satisfy Eqs. (C2). These conditions are satisfied provided that

$$V_1(0)=V_2(0)=0 \tag{C4}$$

$$\lim_{\xi_0\to\infty}[V_1(\xi_0),\ V_2(\xi_0)]=(0,\ 1) \tag{C5}$$

The equations governing the component functions V_1, V_2 are obtained from Eq. (C1) by requiring that the error function ϵ^*, obtained by substituting the form (C3) into Eq. (C1) and evaluating the nonzero right-hand side, be orthogonal to both the basis functions $\sin\tau$, $\cos\tau$. Thus we require,

$$\int_0^{2\pi}d\tau\,\epsilon^*(\xi_0,\tau)\,(\sin\tau)=0 \tag{C6}$$

The limits of integration can be changed from $-\alpha_0\leqslant\tau\leqslant 2\pi-\alpha_0$ to $0\leqslant\tau\leqslant 2\pi$ because of periodicity of the terms appearing in the integrand.

The result of carrying out the integrations indicated in Eq. (C6) is the following set of ordinary differential equations

$$m(d^2V_1/d\xi_0^2)+V_2(V_1^2+V_2^2)^{1/2}=1$$

$$m(d^2V_2/d\xi_0^2)-V_1(V_1^2+V_2^2)^{1/2}=0 \tag{C7}$$

where

$$m=\frac{3\pi}{8}\frac{2}{C_D}\frac{\bar{T}_0(0)/F_0N_D}{(\ell/R(0))^{1/2}}$$

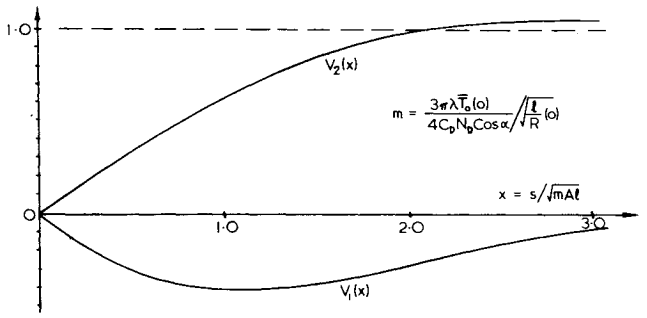

Fig. 6 Boundary-layer displacement components.

It should be noted that the contribution to Eq. (C7) from the dynamic tension, as measured by the expression

$$\int_0^{2\pi} d\tau(\sin\tau, \cos\tau)\{\sin\tau|\sin\tau| \times [\frac{d^2V_1}{d\xi_0^2}\sin\tau + \frac{d^2V_2}{d\xi_0^2}\cos\tau]\}$$

vanishes identically.

Thus, the boundary-layer equation has been replaced by a coupled set of nonlinear ordinary differential equations. The problem remaining is to obtain a solution to this set of equations that satisfies the conditions given by Eqs. (C4) and (C5).

The technique to be followed for solving Eqs. (C7) subject to the end conditions (C4 and 5) involves a combination of a numerical solution and an analytical solution. The numerical solution is obtained using the subroutine RKGS (Runge-Kutta-Gill) mentioned previously, with initial conditions given by Eqs. (C4) and a trial guess for the first derivatives. This solution is required to match an approximate analytical solution, valid for large ξ_0 at a sufficiently large value of ξ_0. This matching is achieved by assuming that the discrepancy between the functions V_1, V_2 and the derivatives $dV_1/d\xi_0$ $dV_2/d\xi_0$ computed both numerically and analytically are functions of the initial estimates for the first derivatives, and used a Newton-Raphson procedure for refining the initial estimate until satisfactory convergence is achieved. The final result, using this procedure, is presented in Fig. 6.

An approximate analytical solution of Eq. (C7) is obtained by assuming, for sufficiently large values of ξ_0, that

$$V_1 = v_1 \qquad V_2 = 1 - v_2$$

and linearizing the resulting differential equations on the assumption that

$$|v_1|,\ |v_2| \ll 1$$

Thus, in terms of a reduced boundary-layer variable x, where

$$x = \xi_0/(m)^{1/2}$$

the equations governing v_1, v_2 become

$$d^2v_1/dx^2 - 2v_2 = 0$$

$$d^2v_2/dx^2 + v_1 = 0 \qquad \text{(C8)}$$

The solution of Eqs. (C8) that dies out as $\xi_0 \to \infty$ is given by

$$v_1 = e^{-ax}(A_1\sin ax + A_2\cos ax)$$

$$v_2 = e^{-ax}(A_2\sin ax - A_1\cos ax)/\sqrt{2} \qquad \text{(C9)}$$

where $a = 1/2^{1/4}$.

The numerical results presented in Fig. 6 were obtained by matching this solution with a numerical solution of Eqs. (C7) at $x = 3.0$. The Newton-Raphson procedure, previously described, essentially fixes the constants of integration (A_1, A_2) by matching the functions V_1, V_2 exactly, and then proceeds to vary the initial conditions $dV_1/dx\,(0)$, $dV_2/dx\,(0)$ until the derivatives $dV_1/dx\,(3)$, $dV_2/dx\,(3)$ obtained both numerically and analytically agree sufficiently well. The constants of integration are never actually calculated, as matching is achieved by comparing slopes and one can verify from Eqs. (C9) that

$$dv_1/dx = -2^{-1/4}(\sqrt{2}\,v_2 + v_1)$$

$$dv_2/dx = (v_1 - \sqrt{2}v_2)/2^{1/4}$$

Alternatively,

$$dV_1/dx = a[\sqrt{2}(V_2 - 1) - V_1) \qquad \text{(C10)}$$

$$dV_2/dx = -[V_1 + \sqrt{2}(V_2 - 1)]\ a^3$$

Thus, given the results of a numerical integration of Eqs. (C7) evaluated at $x = 3.0$, the slopes can be compared directly using equations (C10) without ever evaluating A_1, A_2.

The results presented in Fig. 6 are based on the consideration that the following slope comparisons are adequate.

$$dV_1/dx(3) = 0.1399(\text{RKGS}) = 0.1406 \quad [\text{Eq. (C10)}]$$

$$dV_2/dx(3) = 0.007{,}32\ (\text{RKGS}) = 0.008{,}29\ [\text{Eq. (C10)}]$$

Further refinements to improve agreement were not considered necessary as the purpose of this calculation—to show the plausibility that a solution of Eqs. (C7) exists satisfying Eqs. (C4) and (C5)—seems to have been achieved. Alternatively, should better agreement between derivatives be required, the technique described here, which is essentially a "shooting" technique, should be replaced by a multiple "shooting" technique. This was not undertaken as it seemed pointless to pursue this approach rather than attempting a direct solution of the original partial differential equation, Eq. (38).

References

[1] Casarella, M.J. and Parsons, M., "Cable Systems under Hydrodynamic Loading," *Marine Technology Society Journal,* Vol. 4, July-August, 1970, pp. 27-44.

[2] Choo, Y. and Casarella, M.J., "Hydrodynamic Resistance of Towed Cables," *Journal of Hydronautics,* Vol. 5, Oct. 1971, pp. 126-131.

[3] Berteaux, H.O., "Design of Deep Sea Mooring Lines," *Marine Technology Society Journal,* Vol. 4, May-June 1970, pp. 33-46.

[4] Wilson, B.W. and Garbaccio, D.H., "Dynamics of Ship Anchor-Lines in Waves and Current," *Journal of Waterways and Harbor Division, Proceedings of the ASCE,* Vol. 95, No. W.W.4, Nov. 1969, pp. 449-465.

[5] Langer, R.M., "The Catenary in Space-Free Motions of Flexible Lines," J.R.M. Bege Co., Arlington, Mass., or AD 611429, Defense Documentation Center, Dec. 1964.

[6] Nath, J.H. and Felix, M.P., "Dynamics of Single Point Mooring in Deep Water," *Journal of Waterways, Harbor and Coastal Engineering Division, Proceedings of the ASCE,* Vol. 96, No. W.W.4, Nov. 1970, pp. 815-833.

[7] Chang, P.Y. and Pilkey, W.D., "Static and Dynamic Analysis of Mooring Lines," *Journal of Hydronautics,* Vol. 7, Jan. 1973, pp. 29-34.

[8] Nath, J.H., "Dynamic Response of Taut Lines for Buoys," *Marine Technology Society Journal,* Vol. 5, July-Aug. 1971, pp. 44-46.

[9] Smith, C.E. and Nath, J.H., "Parameters Affecting Natural Frequencies of Buoy, Taut Line Systems," *Marine Technology Society Journal,* Vol. 6, May-June 1972, pp. 49-50.

[10] Paul. B. and Soler, A.I., "Cable Dynamics and Optimum Towing Strategies for Submersibles," *Marine Technology Society Journal,* Vol. 6, March-April 1972, pp. 34-42.

[11] Dominguez, R.F. and Smith, C.E., "Dynamic Analysis of Cable Systems," *Journal of Structural Division Proceedings ASCE,* Aug. 1972, pp. 1817-1834.

[12] McLauchlan, R.A., Sanders, D.R., Taylor, R.D., and Collier, M.L., "A Dynamic Analysis of Moored and Free-Floating Cable Systems," Paper OTC 1742, presented at the 1973 Offshore Technology Conference, April 30-May 2, Houston, Texas.

[13] Breslin, J.P., "Dynamic Forces Exerted by Oscillating Cables, *Journal of Hydronautics,* Vol. 8, Jan. 1974, pp. 19-31.

[14] Wilson, B.W., "Elastic Characteristics of Moorings," *Journal of Waterways and Harbors Division, Proceedings of the ASCE:* Vol. 93, No. W.W.4, Nov. 1967, pp. 27-56.

[15] Clary, G., "Characterization of Ocean Barge Mooring Cables," Rept., May 1973, Harvey Mudd College, Claremont, Calif.

[16] Yamamoto, T., Nath, J.H., and Smith, C.E., "Longitudinal Motions of Taut Moorings," *Proceedings of the ASCE Journal of Waterways, Harbors and Coastal Engineering Division*, Vol. 100, No. W.W.1, Feb. 1974, pp. 35-50.

[17] Cole, J. D., *Perturbation Methods in Applied Mathematics,* Blaisdell, New York, 1968.

[18] Collier, M.L., "Dynamic Similarity Scaling Laws Applied to Cables," *Journal of Hydronautics,* Vol. 6, July 1972, pp. 111-114.